

Density-functional theory study of the effects of atomic impurity on the band edges of monoclinic WO₃

Muhammad N. Huda,* Yanfa Yan, Chang-Yoon Moon, Su-Huai Wei, and Mowafak M. Al-Jassim
National Renewable Energy Laboratory, Golden, Colorado 80401, USA

(Received 18 September 2007; revised manuscript received 18 December 2007; published 6 May 2008)

The effects of impurities in room-temperature monoclinic WO₃ were studied by using the local density approximation to density-functional theory. Our main focus is on nitrogen impurity in WO₃, where both substitutional and interstitial cases were considered. We have also considered transition-metal atom impurities and some codoping approaches in WO₃. We find that, in general, band gap reduction was a common result due to the formation of impurity bands in the band gap. Also, the changes of band-edge positions, valence-band maxima and conduction-band minima, were found to depend on the electronic properties of the foreign atom and their concentration. Our results therefore provide guidance for making WO₃ a suitable candidate for photoelectrodes for hydrogen generation by water splitting.

DOI: [10.1103/PhysRevB.77.195102](https://doi.org/10.1103/PhysRevB.77.195102)

PACS number(s): 71.55.-i, 71.20.-b, 81.05.Hd, 73.20.Hb

I. INTRODUCTION

Production of hydrogen through splitting water under solar irradiation by photoelectrochemical (PEC) process¹ is one of the most promising method, which is, if successful, both cost effective and environment friendly. There has been significant progress in this field using ultraviolet (UV) solar energy.² However, for optimal use of solar energy, the optically visible range of the spectra must be used. To absorb maximum solar energy, the desired photoelectrode must be a semiconductor of band gap around 2.0 eV, and the positions of its band edges must be matched with the water-splitting potential.³ Also, in general, the photoelectrodes must be stable in aqueous solutions. So, to achieve the suitable photoelectrode materials, its electronic properties, and how it responds to the defect formation must be understood

Photochemically, the most stable semiconductors in aqueous solutions are oxides.¹ One of the most popular metal oxides for this purpose, TiO₂, has an indirect band gap of 3.2 eV, which is only suitable for absorbing the UV part of the solar spectrum. To date, shifting its absorbing spectrum to the visible region has not been too successful.⁴ Recent studies have shown that mixing tungsten oxide (WO₃) with TiO₂ can increase the photosensitivity of the electrodes.⁵ WO₃ is well known for its photosensitivity⁶ and its stability against photocorrosion in acidic aqueous solutions. Hence, WO₃, with an experimental direct gap of 2.7 eV,³ is suitable for efficient use as photoelectrodes⁷ and other optoelectrical devices. The photon-absorbing property of these oxides in the visible range can be improved by tuning its bands to the proper gap and placing the band edges in the desirable position, such as raising both the valence band and conduction band edges.⁸ One way of doing this is to add impurity to the materials, such as nonmetals (e.g., nitrogen or carbon atoms) or metals, or to codope with both types of atoms. It has been shown before that, for example, in the case of TiO₂, the incorporation of N reduces the band gap and shifts the absorption spectra toward the longer-wavelength photons.^{9,10}

Here, we briefly mentioned other studies on the doping of WO₃ for PEC purpose. Mg doping in WO₃ was experimentally studied by Hwang *et al.*¹¹ They showed that Mg-doped

WO₃ has a band gap similar to undoped WO₃, but the conduction-band minimum moves up to match the H⁺/H₂O potential. In another combined experimental and theoretical study, Tang and Ye¹² showed that Bi₂W₂O₉ is also capable of spontaneously producing hydrogen from an aqueous CH₃OH solution under visible light. Doping with other metals (e.g., Cu and Ag) was also reported in the literature^{13,14} without much success. A recent experiment by Paluselli *et al.*¹⁵ showed that nitrogen-doped WO₃ has a smaller band gap; also, the transmission spectra have a blueshift due to the incorporation of N atoms. This study found that the band gap of the WO₃ thin film was significantly reduced, almost by 0.8 eV as the N atoms increased. From this large band gap reduction, one can infer significant nitrogen atom concentration in the film. Also, with increasing N-atom concentration, the absorption spectra shifted toward the longer wavelength region. It should be mentioned that a higher concentration of N atom than as defined by the “doping regime” in the host materials can be achieved by proper growth condition manipulation, such as changing the chemical potential of the impurity atoms.^{16,17}

In this paper, we present *ab initio* theoretical studies on various impurities in WO₃ and their electronic properties. One of our main focus is on N impurity in WO₃ in the room-temperature monoclinic phase. Substitutional and interstitial impurities were both considered. We found that a certain type of interstitial nitrogen is more preferable than substitutional nitrogen to achieve the PEC properties, although the formation of these defects strongly depends on the growth condition. However, it was found that although absorption at the longer wavelength is increased by N impurity in WO₃,⁷ the photocurrent did not appreciably increase. One reason might be that the recombination centers are created by the charged defects. Isovalent codoping usually improve the situation. For this reason, we have also considered transition-metal atom impurities and some codoping approaches in WO₃. In general, the uplift of valence-band maxima can be achieved by incorporating metals with *d* bands shallower than tungsten. In this paper, only the metal atoms around W in the Periodic Table are considered to minimize the size and chemical mismatch. Other isovalent impu-

TABLE I. Atomic orbital eigenvalues (in Ry) of dopant atoms along with W and O atoms are listed to show the general chemical trend (Ref. 18).

Atom	<i>s</i>	<i>p</i>	<i>d</i>
B ($2s^2 2p^1$)	-0.690	-0.273	
N ($2s^2 2p^3$)	-1.354	-0.532	
O ($2s^2 2p^4$)	-1.746	-0.676	
Al ($3s^2 3p^1$)	-0.575	-0.204	
Mo ($5s^1 4d^5 5p^0$)	-0.318	-0.086	-0.289
Hf ($6s^2 5d^2 6p^0$)	-0.382	-0.108	-0.215
Ta ($6s^2 5d^3 6p^0$)	-0.413	-0.109	-0.278
W ($6s^2 5d^4 6p^0$)	-0.434	-0.108	-0.344
Re ($6s^2 5d^5 6p^0$)	-0.453	-0.106	-0.409

rities were also considered, such as Mo in place of W or (NH) in place of O. Table I shows the eigenvalues for atomic *s*, *p*, and *d* orbitals for the dopant atoms along with W and O atoms. This gives us an initial guidance as what to expect upon doping of these atoms and will be discussed later in this paper. We expect that this spectrum of impurities would provide a clearer picture of the trend of band-structure modification of WO₃.

II. COMPUTATIONAL METHODS

For the total energy calculation, we used the local density approximation¹⁹ (LDA) to density-functional theory with the projected augmented wave (PAW) method,^{19,20} as implemented within the Vienna *ab initio* simulation package (VASP 4.6.21).^{21–24} Because of its construction, the PAW method is believed to agree with the all-electron results better than the results by ultrasoft pseudopotentials. One reason is that PAW potentials reconstruct the exact valence wave function with all nodes in the core region. The reason for choosing LDA is that it agrees better with the experimentally measured volume for WO₃. The relaxed lattice constants are $a=7.381$ Å, $b=7.472$ Å, and $c=7.633$ Å. These numbers compares well to the similar LDA calculations by de Wijs *et al.*²⁵ The experimental lattice constants are 7.306, 7.540, and 7.692 Å. All plane waves with a cutoff energy of 400 eV were used in the basis function, and the Brillouin zone (BZ) integrations were performed by using the second-order Methfessel–Paxton method.²⁶ The room-temperature monoclinic structure of WO₃, with 32 atoms in the unit cell, was considered for our calculations, unless a larger unit cell was needed. For example, to study a very dilute regime, or antiferromagnetism, a 64-atom unit cell was used. The lattice constants (and volume) of the WO₃ were optimized. These lattice constants were kept fixed throughout our calculations. However, the ion positions were always relaxed until the force on each of them is 0.01 eV/Å or less. For ion relaxation, $2 \times 2 \times 2$ Monkhorst–Pack²⁷ *K*-point sampling was used; however, for density-of-states (DOS) plots, a more refined $8 \times 8 \times 8$ *K*-point sampling was used.

III. UNDOPED WO₃

The smallest monoclinic unit cell of WO₃ consists of 8 W atoms and 24 O atoms. The monoclinic WO₃ can be consid-

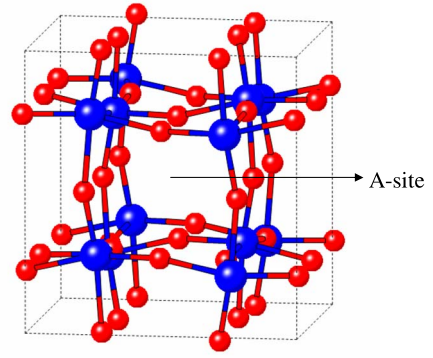


FIG. 1. (Color online) The monoclinic structure of WO₃ unit cell is shown here. W and O atoms are represented by the blue (dark) and red (gray) balls, respectively. The perovskite A site as in ABO₃ is shown.

ered as a deformed perovskite structure, like ABO₃ where the A ions are missing and B is replaced by W.²⁸ These A positions, as shown in Fig. 1, are suitable for interstitial doping. The WO₃ structure can also be considered as consisting of W-O-W-like chains, where the chains are connected across the W atoms, as seen in Fig. 1. This pseudo-low-dimensional structure of WO₃ has given rise to many interesting properties, including superconductivity.²⁹ From the band structure in Fig. 2, we see that there are two nearly degenerate states at the conduction-band minima (CBM). The valence-band maxima (VBM) states at Γ point (folded from the *R* point of the undistorted cubic cell) also split due to the slight distorted arrangement of the octahedrons. Also, at $B \rightarrow \Gamma$, the top of the valence band is flat. This dispersionless band indicates very high effective masses for the holes along the W-O-W chain in the *x* direction, which constitutes tightly bound corelike electronic behavior along that direction on the zone boundary. Similar high effective masses were found for electrons in the $\Gamma \rightarrow Z$ direction. This has some interesting consequences in electronic behavior of WO₃, such as conduction being highly prohibitive in those directions. Besides these flat bands, there is also a highly dispersive part of the bands along other symmetry points at the Fermi level. This simultaneous presence of highly dispersive and nondispersive bands around the Fermi level indicates the potential of superconductivity.^{30,31} Figure 2(b) shows the total and local DOS. The sharp rise of the valence-band DOS at the Fermi level is due to the flatbands found in the band structure. The local DOSs are amplified for clarity. This shows that, as expected for a metal-oxide semiconductor, the valence band of WO₃ mainly consists of O *p* bands, while its conduction band has predominantly W *d* character. In fact, the onset of *p*-*d* hybridized band density in the valence band starts from 0.6 eV below the Fermi level, where the Fermi level is located at the top of the valence band. The band gap was found to be pseudodirect at the Γ point and is 1.31 eV, which is much less than the experimental band gap of 2.6 eV. This underestimation of band gap is a consequence of the LDA used in our calculation. Reference 25, employing VASP and ultrasoft pseudopotentials, has also found a direct LDA gap of 1.1 eV. Because we are mostly concerned with the

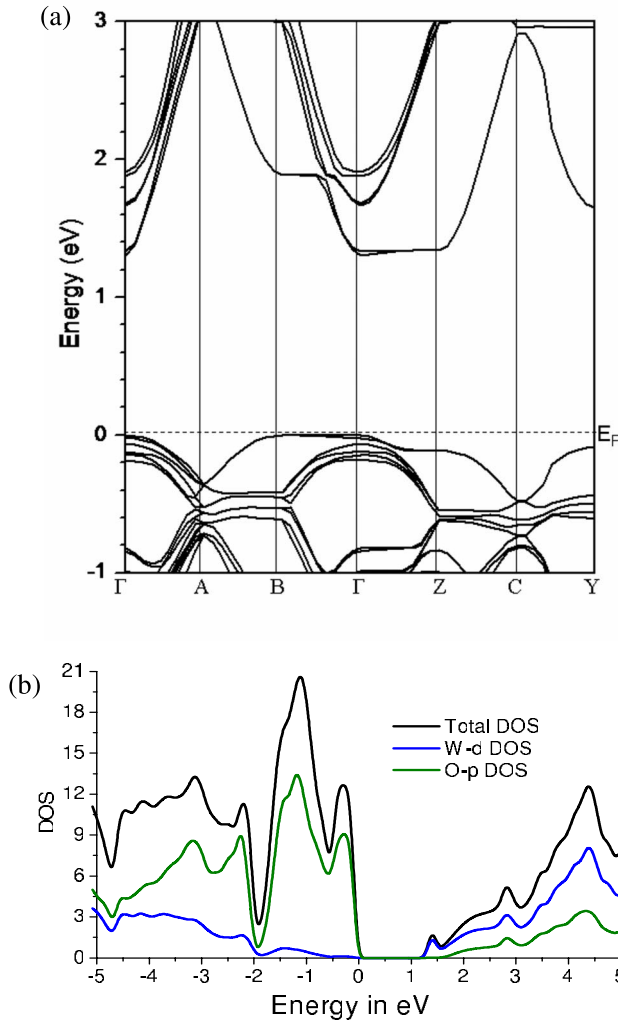


FIG. 2. (Color online) (a) The band structure plot is shown along the high-symmetry points and (b) DOS for both total and site and angular momentum decomposed local DOS plots for monoclinic WO_3 . The top of the valence band is set to 0 eV. Partial DOS plots are amplified several times for better visibility.

relative energy changes between different impurity states, we expect that this computational underestimation would not significantly affect our results.

IV. NITROGEN IMPURITY

A. One nitrogen atom substitution

We first discuss one nitrogen atom substitution in the WO_3 unit cell. The nitrogen atom replaced one of the 24 oxygen atoms in the unit cell, which gives $\sim 4\%$ N impurity. Substitution of a nitrogen atom is not expected to cause significant changes in structural or bonding properties because the size mismatch is minimal and the difference in electronegativity is small. From Table I, we can see that the energy of N p orbital is higher than the O p orbitals' energy. This implies that upon substitution of O in WO_3 , the N p band would be above the valence-band maxima, which mainly

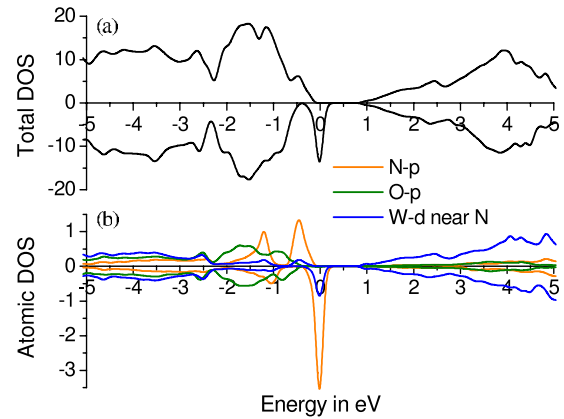


FIG. 3. (Color online) (a) Total DOS and (b) local DOS for WO_3 with 1 O out of 24 atoms substituted by a N atom. The Fermi levels for all of the DOS plots here are set to zero. A high density of states of half-filled N $2p$ band is clearly seen at the Fermi level. O $2p$ DOS, which is located far from the N atom, started below -0.40 eV and is almost unaffected by the presence of the N atom.

consists of O p . As can be seen from the total DOS plot in Fig. 3(a), the one less electron in the N atom compared to the O atom introduces a hole in the valence band as an extra carrier, which may increase the conductivity of the system as a p -type semiconductor. Also, due to this unpaired electron at the Fermi level, the system becomes spin polarized. From the total DOS plot, one can see that there are partially filled bands at the Fermi level for the minority spin, which could initiate an ordering of long-range collective magnetic moment. The non-spin-polarized system was found to be 0.082 eV higher in total energy than the ferromagnetic arrangements. The partial DOS in Fig. 3(b) shows that, as expected, the partially filled bands are primarily from the N p states. These N p bands are hybridized with the neighboring O p bands, and very slightly hybridized with the nearest W d bands. So, the top edge of the valence band is mainly composed of the p bands, as was the case of pure WO_3 , but mainly from the nitrogen atom. Oxygen atoms in the cell that are located further from the N atoms are somewhat unaffected by the presence of N atoms, as can be seen from their O p bands, which are also shown on the p -DOS plot. These unaffected O p bands started from 0.40 eV below the Fermi level. This indicates that the top of the valence bands of WO_3 can be raised up in energy due to the N substitution. The band structure (Fig. 4) shows that although the occupied spin-up bands are all below the Fermi level, two spin-down bands are situated around the Fermi level and at a distance of 0.2 eV from the other part of the valence band. At the Γ point, both of these two spin-down bands are unoccupied and mainly have a N p character. At the BZ boundary, from K -point $B \rightarrow \Gamma$, the top of the valence band is no longer dispersionless, as it was in pure WO_3 , which indicates that the presence of nitrogen initiates further electron interactions within neighbors in the x direction. However, the dispersion is not very significant on the top of the valence band; consequently, in the case of the spin-down band, the holes would not experience much influence from the neighboring atoms. Also, the band gap is reduced from 1.31 to 1.04 eV for the

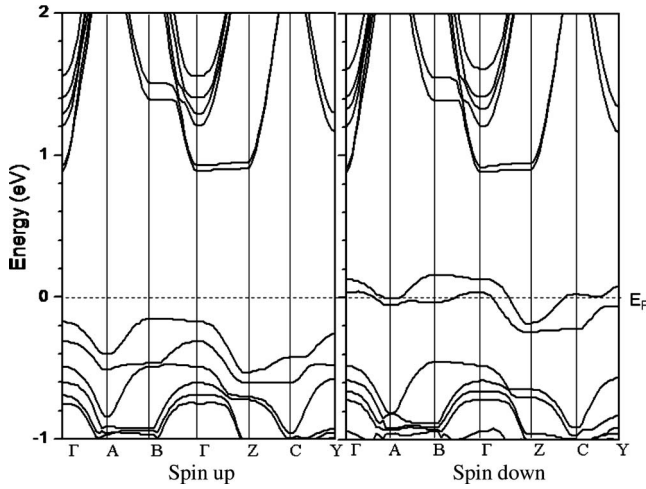


FIG. 4. Band structure for both up and down spins of WO_3 with an O atom substituted by an N atom. For spin down, partially filled bands are seen around the Fermi level.

spin-up bands and 0.89 eV for spin-down bands. Table II listed modified band gaps due to the impurity in WO_3 . However, these types of systems with large partially filled DOS at the Fermi level are unstable, and further relaxation with a larger supercell showed that a gap opens up in the spin-down bands and the system became a semiconductor with a band gap of 0.5 eV with ferromagnetic behavior. Magnetism in this situation poses a very interesting problem. This is beyond the scope of the present paper and will be discussed elsewhere.³³ In our calculation, we found that although the pure WO_3 gap is direct, N-substituted gaps are indirect; for spin-up bands, it is $B \rightarrow \Gamma$. Also, the conduction-band edge, which is mainly composed of W d electrons, changes position by 0.09 eV upward, while the VBM shifts up by 0.51

TABLE II. Band gaps in eV are listed for WO_3 with impurities. For spin-polarized systems, both the spin-up and the spin-down band gaps are listed. For undoped WO_3 , the calculated band gap is 1.31 eV.

Dopants	Band gaps (eV)
N_O	1.04, 0.89
2N_O	0.84
N_i	0.78, 0.63
$(\text{N}_2)_i$	1.53
$(\text{N}_2)_i + \text{N}_i$	0.60
$(\text{N}_2)_\text{O}$	1.24
$(\text{B-N})_\text{O}$	0.88
Al_W	1.26
Mo_W	1.32
Ta_W	1.21, 1.12
Hf_W	1.23, 1.07
$(\text{Re-N})_{\text{W-O}}$	1.03
$(\text{Ta-F})_{\text{W-O}}$	1.21
$(\text{N-H})_\text{O}$	0.89

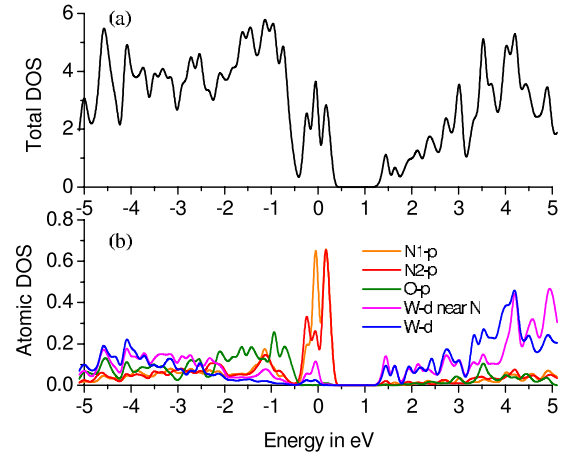


FIG. 5. (Color online) (a) Total DOS and (b) site and angular momentum projected atomic DOSs for 2N substituted WO_3 .

eV. Here, the band-edge shifts are calculated with respect to the O s core level away from the impurity N atom. Hence, the band edges (VBM and CBM) as a whole slightly shift upward. In short, substitution of N for O in WO_3 changes the VBM toward higher energy, but the CBM does not change much; as a result, the band gap decreases.

B. Two nitrogen atom substitution

Next, we doubled the substitutional impurity level to 8%, i.e., two O atoms were substituted by two N atoms in a WO_3 unit cell. Among the several 2N substitutional options, the lowest-energy one was found when the two N atoms resided at the two closest O substitutional sites. As a result, two N atoms were on two crossed O-W-O chains. At these sites, the N-N distance is 2.51 Å and the N-W-N angle is $\sim 87.10^\circ$. These parameters are not significantly different from those of the pure WO_3 structure; however, the N-N distance is 0.12 Å closer than the shortest O-O distance. To see if this two-N-atom substitution is favorable, we calculated the binding energy of this 2N substitution formation by the following definition:

$$E_b = E_{\text{tot}}[\text{WO}_3 + 2\text{N}_\text{O}] + E_{\text{tot}}[\text{WO}_3] - 2E_{\text{tot}}[\text{WO}_3 + \text{N}_\text{O}], \quad (1)$$

where E_{tot} is the total energy of the system defined. Here, negative binding energy would indicate that the particular formation is possible. We find that this two-N binding energy is -0.76 eV, indicating that the pair formation is favorable in this case, but not very strongly. From the l -projected atomic DOS [Fig. 5(a)], one can see that there is a hybridization of W d and N p bands near the Fermi level, and this, unlike pure WO_3 , attributes some d character to the valence-band edge. The W atom connecting the two N atoms loses some charge to the N atoms, and the overall system was nonmagnetic. This gives the almost similar conduction-band edge as the undoped WO_3 , although the splitting at the bottom of the conduction band was increased. For this system, the VBM significantly moved up in energy, with an empty band just above the Fermi level, which may contribute extra

holes at the valence band. The probability that this empty band near the Fermi level would facilitate the absorption process is low because this band as well as the top of the occupied band is mostly composed of p bands. Only a tiny portion of d band DOS exists near the Fermi level. So, the optical band gap here would be the difference between the top of the occupied band and the bottom of the conduction band. This band gap is the least at the Γ point, 0.84 eV, which is significantly reduced from the pure WO_3 band gap. The relative position of the top of the occupied band shifted up by about 0.45 eV, and the band gap is reduced because the CBM shift is not as much as the VBM. Although the distortion, both structural and electronic, is higher, this impurity level due to the uplift of the VBM may be useful for optical absorption at the visible range.

The other higher-energy 2N-substituted structures need to be mentioned here. For example, two N atoms on the same chain or in the adjacent chains differently behave. The two N atoms on the same chain go through some type of charge-density instability, become spin polarized, and the empty $N p$ bands sit below the spin-down conduction band. Although not significant, this also causes the conduction band to slightly increase in energy. On the other hand, if two N atoms are on two adjacent chains, the system becomes non-magnetic, with small ($\sim 0.025\mu_B$) but opposite moments on the N atoms. Here, also, there is a half-filled DOS peak around the Fermi level and empty bands above the Fermi level. This would also create a semimetallic behavior. However, the band gap reduction is not as large as the previous one, 1.30 eV, which is almost similar to the undoped WO_3 .

On the other hand, reducing the N-atom concentration down to 2 at. % shows that the previously partially filled spin-down band at the Fermi level (i.e., at 4 at. % impurity) now became completely empty, less dispersive, and comprises of hybridized $N p$ and $O p$ bands. Here, the electron concentration at the Fermi level is very low and consists of spin-down electrons. Spin-up electrons are 0.1 eV below the Fermi level. So, the pseudometallic conduction behavior, which was apparently found at the 4% impurity level, has vanished at this lower concentration. Strong exchange splitting at the $N p$ bands occurs above the unperturbed $O p$ bands. This apparently pushes the conduction band slightly higher than it was before without N atoms. The difference in energy of the CBM between the 2 at. % N impurity and undoped WO_3 is 0.2 eV. Overall, due to N substitution, the band gap does decrease as the valence band rises. However, only at lower (2 at. %) and higher (8 at. %) concentrations, the conduction band moves upward, while at 4 at. % N concentration, where one O atom is replaced by one N atom in a unit cell, the CBM remained unaffected.

C. Interstitial N

For a single interstitial nitrogen atom, the character of the CBM considerably changes. The interstitial N atom is mainly bonded with the O atom with a bond length of 1.31 Å, and the nearest W-N bond length is 2.03 Å. This can be considered as a NO molecule substituted for an O atom. As seen from the atomic DOS plot [Fig. 6(b)], the $N p$ impurity band

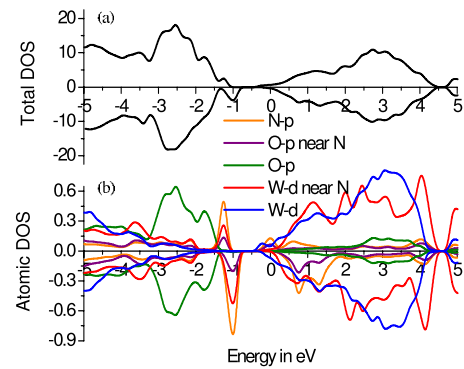


FIG. 6. (Color online) A N-atom interstitial in WO_3 : (a) total DOS and (b) site and angular momentum projected atomic DOS.

is now just below the conduction band. This impurity band is hybridized with O p and W d bands and is partially filled for the spin-up electrons. This also makes the W d band in the conduction band spin polarized and partly filled with very small exchange splitting. For the spin-down bands, unlike spin-up bands, the bottom edge of the conduction band does not have any N -like character; rather, it is mostly a d -like band and partially filled. The system here is now more conducting because some electrons are available in the conduction bands; as a result, this interstitial N can be considered as a donor. A larger supercell calculation showed that it prefers antiferromagnetic behavior. The fundamental gap³² is decreased further, 0.78 and 0.63 eV for spin up and spin down, respectively. For spin up, the band gap is indirect ($\Gamma \rightarrow Z$); however, the direct band gap (at Z) is only 0.01 eV higher. In both cases—spin up and spin down—the CBM at these symmetric K points has W d -like character. Note here that although the VBM rises in energy, there is no significant change in the position of CBM because the unoccupied molecular orbital of NO is higher than CBM.

D. More than one interstitial nitrogen atoms

To explore other possibilities further, we considered impurity in a WO_3 unit cell with more than one interstitial N atom. For two interstitial N atoms, the lowest-energy structure has no longer N atoms attached to the O atoms; rather, the two N atoms formed a dimer in the hollow space of the WO_3 unit cell, which is the A site if we consider the perovskite ABO_3 structure (Fig. 1). The total energy difference between these two configurations—dimer in a hollow space and 2N bonded to two O atoms—is quite large, 5.094 eV. This strongly indicates the favorable environment for the interstitial N-N dimer formation. As expected, the N_2 dimer formed a closed shell with N-N bond length of 1.10 Å, and the overall magnetic moment is zero. The nearest N-W and N-O distances are 2.90 and 2.41 Å, respectively. As a result, along with the fact that N_2 is known for not binding an extra electron,³³ the interaction with the O or W atoms with this N_2 dimer is not very strong. The top of the valence band, like WO_3 , consists of O p bands, whereas the $N p$ band sits inside the O p bands with weak hybridization (Fig. 7). Overall, although the total DOS has a similar feature at the band edges as in the pure WO_3 total DOS, the position of the

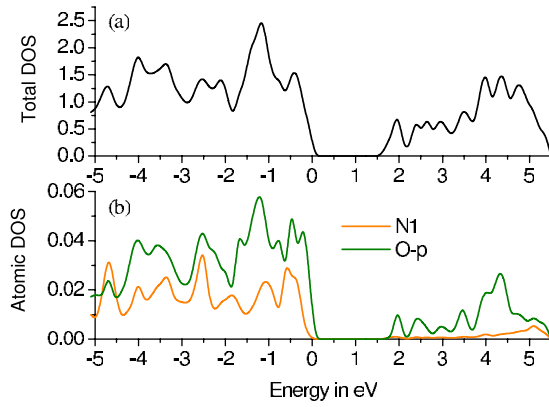


FIG. 7. (Color online) Total and site and angular momentum projected atomic DOS plots for two interstitial N atoms in WO_3 . These two N atoms formed a dimer in the hollow site (A site) of WO_3 .

conduction-band edge moved up by almost 0.35 eV. As a result, the total band gap increased to 1.53 eV, which is higher than the undoped WO_3 band gap. The structural deformation of the lattice due to N_2 at an A site, rather than charge transfer to or from N, which is negligible here, is responsible for the band gap increase. This increase in band gap would mark this configuration as an undesirable one. However, an upward shift of the conduction band tends to reduce the overpotential, which is favorable for the photoelectrodes. So, further careful impurity addition, which may reduce the band gap, needs to be examined. One of the examples will be discussed in the following paragraph. As a passing comment, putting a N atom at the A site does not yield a lower-energy structure due to the unstable nature of a lone N atom.

For three interstitial nitrogen atoms, several configurations were considered, including the one with 3N bonded with three O atoms. This particular configuration greatly distorts the WO_3 structure, with several eV higher in total energy than the most favorable one in our calculation. The ground-state configuration for three N interstitial atoms occurs when two N forms a dimer at the A site, as before for 2N interstitial, and the third N atom is attached to one of the oxygen atoms. Here, also, the binding energy for the N-N dimer formation in a cell with one N interstitial attached to O atom is high, -4.26 eV. As before, the N-N bond length remains the same (1.10 \AA), but the N-O bond length slightly increased to 1.44 \AA , compared to the N_2 interstitial and single N interstitial configurations, respectively. The DOS at the Fermi level has the similar feature as the one with the single interstitial N atom; also, there are partially filled bands near the conduction bands, with relatively higher density of states, which are clearly visible in the total DOS plot (Fig. 8). Hence, at this higher impurity level, the system may show more conducting behavior with higher electron concentration near the conduction band. Also, the two peaks on top of the valence bands are now separated slightly more than the single N interstitial DOS. For up spin, the gap between the occupied and unoccupied bands is less than 0.2 eV, whereas for down spin, a tiny part of the band is populated by electrons with no apparent gap with the conduction-band con-

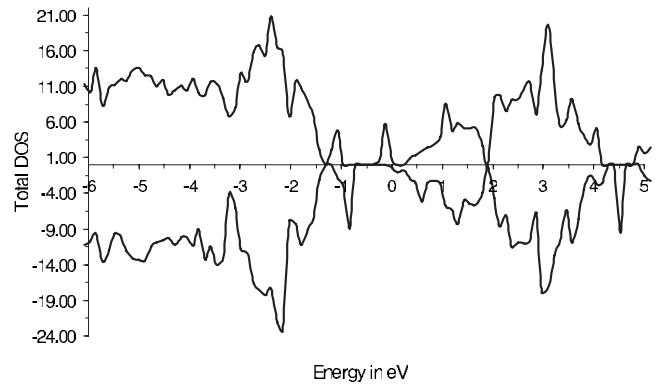


FIG. 8. Total DOS plot of WO_3 with three interstitial N atoms, where 2N forms a dimer at the A site, and the other N atom is bonded with an O atom.

tinuum. So, conduction in the minority spin is highly suppressed. Below the occupied part, the up- and down-spins have a similar band gap of ~ 0.6 eV. The shift of VBM and CBM is significantly larger in this case. The top of the valence band and the minimum of the unoccupied conduction band increase in energy by 0.7 and 0.3 eV, respectively. This large band-edge movement is due to the structural deformation and to the impurity-band effect, as discussed for N atom and N_2 interstitial impurity. This large change of the band position may facilitate the optical absorption at the visible spectrum from solar radiation to split water molecules. It should be emphasized that due to multiple peaks in the fundamental gaps, it may also be used to absorb the shorter wavelength of the solar spectrum. Hence, better control could be achieved by addition of optimal nitrogen impurity in WO_3 . Just as single interstitial N atom in WO_3 gives rise to antiferromagnetism, it is more likely here as well. In this case, the conduction band would be populated with electrons of both types of spin, canceling any long-range magnetic effect.

E. Split interstitials

So far, we found that substitutional and interstitial N impurities create *p*- and *n*-type WO_3 , respectively, and that placement of a N_2 dimer in the hollow spaces can uplift the band edges toward higher energy. Next, we consider the split-interstitial case, i.e., one oxygen atom in WO_3 is replaced by two N atoms. The N-N bond length in the present configuration is 1.19 \AA ; hence, two N atoms are, in reality, behaving like a N_2 molecule. Unlike the N_2 dimer in the hollow space, both N atoms here are bonded with W atoms. Hence, in the present case, N *p* and W *d* hybridizations are expected to be stronger. The binding energy for the $(\text{N}_2)\text{O}$ is calculated by

$$E_b = E_{\text{tot}}[\text{WO}_3 + (\text{N}_2)\text{O}] + E_{\text{tot}}[\text{WO}_3] - E_{\text{tot}}[\text{WO}_3 + \text{N}_\text{O}] - E_{\text{tot}}[\text{WO}_3 + \text{N}_\text{i}], \quad (2)$$

where $E_{\text{tot}}[\text{WO}_3 + \text{N}_\text{i}]$ is the total energy when interstitial N is bonded with an O atom. The binding energy was -4.65 eV, which is slightly lower than the dimer formation in the hol-

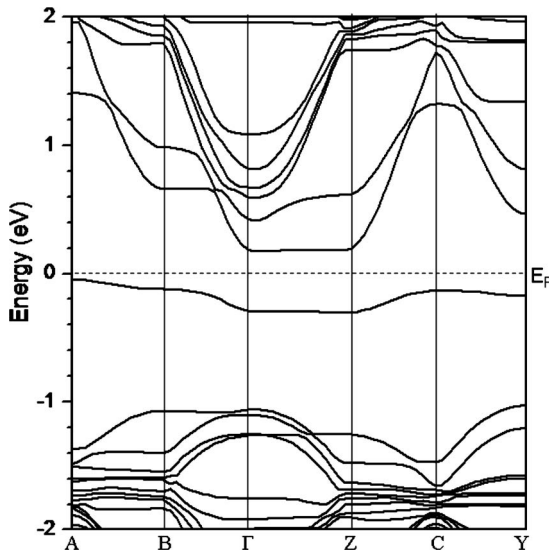


FIG. 9. Band structure of 2N split interstitial in WO_3 along some high-symmetry K points. Also, the Fermi level is set to zero here.

low site, but it is definitely more favorable than the substitutional or separated interstitial defect formation. As seen from the band diagram in Fig. 9, an occupied band is situated in the middle of the gap that is mainly composed of N p and W d bands. Compared to NO substitution, as discussed earlier, N_2 substitution has one electron less, which explains the not-so-populated conduction bands as in NO substitution. However, due to direct N p and W d hybridizations, this particular band is located near the conduction band, and its dispersive nature reflects the influence of the WO_3 CBM. The minimum direct gap from fully occupied to unoccupied bands is only 0.468 eV, whereas the indirect gap is much smaller (0.220 eV). Due to coupling of the unoccupied N_2 molecular orbital, the minimum of the unoccupied conduction band slightly decreased in energy. From the local DOS [Fig. 10(b)] plot, one can also see that the valence band slightly increases compared to the pure WO_3 valence band. The gap from the valence band to the conduction band is

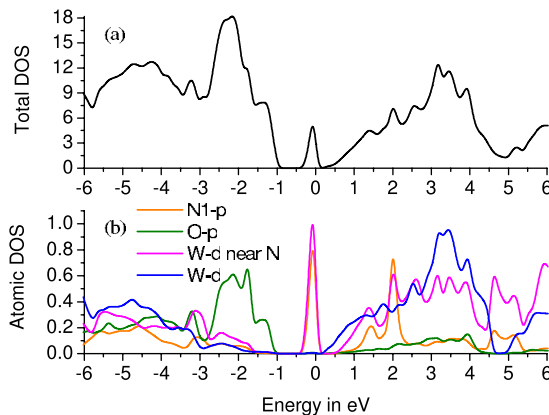


FIG. 10. (Color online) Total and local DOS plots for 2N-split interstitial in WO_3 . Intermediate-band-like formation is clearly visible in the band gap.

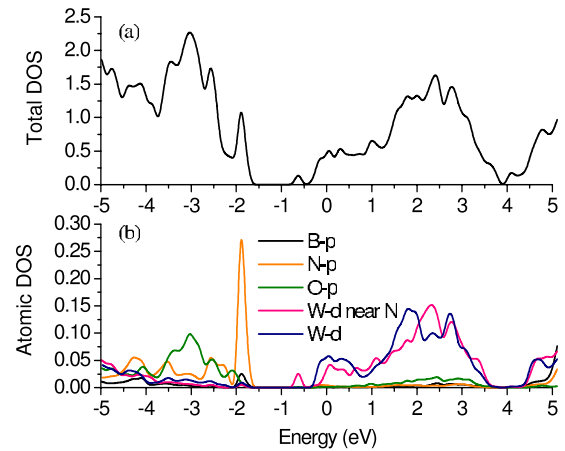


FIG. 11. (Color online) Total and site and angular momentum projected atomic DOS plots for B-N substitution in WO_3 .

1.235 eV, which is slightly less than the undoped WO_3 gap. So, except for the presence of the impurity donor band, the relative changes in the bands are not significant. Also, the possibility is low that the impurity band may act as a stepping stone for the low-energy optical absorption because it is completely filled. Similarly, two split interstitials on the same cell introduce two similar fully occupied impurity bands, which are situated very close to the conduction band; as a result, the bands are highly dispersive and the system becomes almost metallic. Here, the impurity-band width is 0.73 eV, which is 0.48 eV higher than that of the single split-interstitial impurity, and the fundamental band gap is 1.26 eV. Also, in this case, the bottom of the conduction band is heavily hybridized with the N $2p$ band and the impurity band becomes almost a part of the conduction-band continuum. So, the relatively higher width of the occupied impurity band would be responsible for the extra electron in the conduction band at minimum thermal excitation.

To further see the effect of a split interstitial, a B-N dimer was also tested because it forms very strong bonds, similar to a carbon dimer with extra ionicity and higher electronegativity than N_2 . The B-N dimer was put in the WO_3 unit cell by replacing an oxygen atom. The relaxed bond length of B-N was found to be 1.38 Å. The valence-band edge shifted upward by 0.57 eV, whereas the conduction band's upward shift is only 0.16 eV compared to the pure WO_3 bands. The fundamental gap of this structure is reduced to 0.88 eV. In Fig. 11, we see the l -projected atomic DOS plot. In this case, the impurity band, mainly composed of N $2p$ bands, lies above the WO_3 conduction band. The Fermi level goes through the conduction band, and it becomes an n -type semiconductor. A similar feature was found for the spin-down interstitial N impurity. However, for B-N substitution, the W d band closest to the B-N shows higher density of states at a lower energy than the other W d bands. This indicates that the lower part of the conduction band would be heavily influenced by the B-N substitution.

Overall, N_2 substitution for O in WO_3 introduces dispersive fully occupied impurity bands in the gap. Also, although it does not introduce any carrier into the conduction band, the closeness of the impurity band to the conduction band

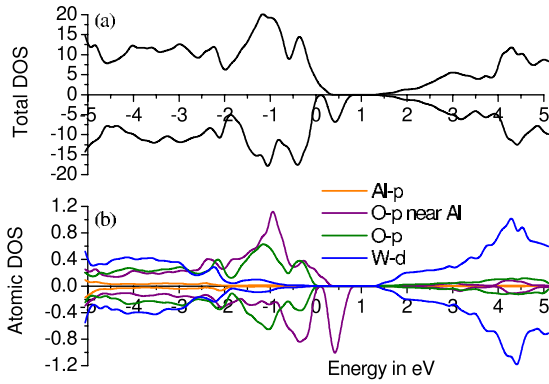


FIG. 12. (Color online) (a) Total DOS and (b) site and angular momentum projected atomic DOSs for Al-substituted WO_3 .

may provide some electrons in the conduction band from the impurity band with slight perturbation. Increasing the electronegativity by replacing N-N with B-N, we found that the band edges noticeably uplift. This also put some carriers at the bottom of the conduction band.

V. METALLIC ATOM SUBSTITUTIONS

Metal substitution in WO_3 would replace W atoms, which are sixfold coordinated, with O atoms. So, metal atoms with shallower d bands in place of W atoms would push up the CBM. Let us first consider the substitution of a simple metal, Al, which has no d orbitals, in WO_3 . Al substitution in place of W atoms results in a highly mismatched condition. First, Al's p orbitals have some contribution deep in the valence bands, which may not have a significant effect on the valence-band edges. Also, from Table I, we see that the Al p orbital is higher in energy than W d orbitals, which may imply that the conduction-band minima would be unaffected by the Al substitution. However, because Al is coordinated with six oxygen atoms, where both types of atoms are of similar size, a local lattice relaxation around the Al atom has been observed that smoothes the W-O-Al chain to almost a straight line. Also, because Al lacks d electrons, the d bands in WO_3 remained almost unaltered (Fig. 12). For example, the onset of the W d band in the valence band is 0.6 eV below the Fermi level for both the Al-doped and undoped WO_3 (Fig. 12). Also, the conduction band, which mainly consists of W d bands, did not change its position. On the other hand, although the O p band did hybridize with the Al p bands, the major contribution to the valence bands here also comes from O p bands. There are hole states above the Fermi levels that are also mainly composed of O p bands, as expected, due to the lack of valence electrons. The loss of electrons in the valence band due to Al substitution is the reason for VBM uplift. The empty states in the spin-down bands are almost like intermediate bands, which are created due to the large size and chemical mismatch between W and Al atoms. However, as the valence-band edge and these empty intermediate bands are both mainly made of O $2p$ orbitals, the transition probability would be very low between these bands. Hence, these empty bands may not facilitate the optical absorption process. Apart from creating these

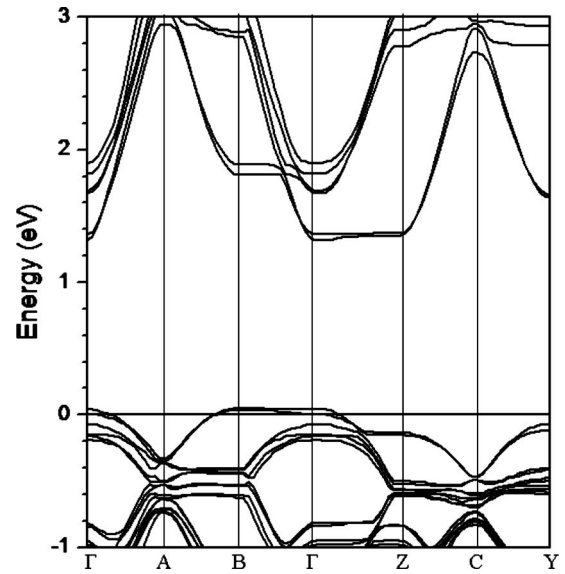


FIG. 13. Non-spin-polarized band diagram for Mo-substituted WO_3 .

hole impurity bands, Al substitution did not significantly change the WO_3 electronic structure.

Next, we consider transition-metal substitution and its effect on the electronic structure of WO_3 . Only those metals around W in the Periodic Table were considered to minimize the size mismatch. These metals vary only in the number of s and d electrons in their valence band, so the strength of hybridization with O p bands varies and the conduction-band minima are also likely to be affected.

Let us first consider Mo substitution, which is isovalent to W. Because W and Mo are in the same column of the Periodic Table, with Mo just above W, one would expect that their electronic properties would not significantly change. In addition, their electronegativity differs by only 0.20. So, this substitution would not provide extra ionicity in the crystal, and the band positions and band degeneracy would likely remain the same. From the band diagram, one can see that the band profile of Mo-substituted WO_3 remains the same as undoped WO_3 , except for a partly unoccupied Mo s band just around the Fermi level (Fig. 13). This is probably due to the fact that, as can be seen from Table I, the atomic Mo s orbital is higher in energy than the W d and O p orbitals. Except for this s band, the VBM and CBM remain the same, with a band gap of 1.32 eV, which is almost the same as for pure WO_3 .

Next, we consider the substitution of Ta and Hf atoms for W atoms. The main reason is that they have shallower d bands compared to W (Table I), which would form d bands at a higher energy in the conduction bands. For Ta atom substitution, two facts need to be considered: first, Ta has only one less $5d$ electron compared to the W atom; second, Ta differs in electronegativity by 0.86 from W. So, the substitution of Ta for W creates extra ionicity in the crystal and removes the apparent degeneracies from the band edges. Hole states are present on top of the valence band, as can be clearly seen from the atomic DOS plot (Fig. 14). The band gaps were 1.21 and 1.12 eV for the spin-up and spin-down

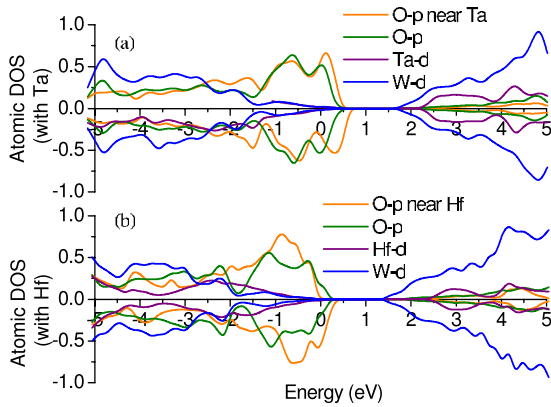


FIG. 14. (Color online) Site and angular momentum projected atomic DOS plots for (a) Ta-substituted and (b) Hf-substituted WO_3 .

bands, respectively. Here, the reason for the band gap reduction, for example, in the spin-down channel, is that the valence band increased in energy by 0.1 eV. The valence-band edge consists of O *p* bands, which are near the Ta atom, as expected. Interestingly, the onset of partial DOS of hybridized *d* bands from both W and Ta atoms starts almost from the same place just below the Fermi energy, whereas for WO_3 , it starts from 0.6 eV below the Fermi level. The CBM remained almost the same, decreasing by less than 0.09 eV. However, the Ta *d* bands were formed about 0.6 eV behind the conduction-band edge, which is expected from atomic *d* orbital energies in Table I. This indicates that with optimal Ta substitution, the conduction band could also be slightly raised.

Similarly, compared to a W atom, Hf has 1.06 less electronegativity and two fewer 5*d* electrons, and one would expect a greater change in the WO_3 structure. For example, exchange splitting in the O *p* bands bonded to the Hf atom is

higher; as a result, the hole states are broader in the spin-down band. Also, the *d* orbital of the Hf atom lies at a higher energy than the W *d* orbital (as in Table I), which is also reflected in the conduction band: the Hf *d* band formed about 1 eV above the W *d* band. However, the band gap decreases to 1.23 and 1.07 eV, respectively, for spin-up and spin-down bands. So, the spin-up band gap increases and spin-down band gap decreases slightly compared to the Ta substitution. Higher exchange splitting in Hf substitution is responsible for this phenomenon. Also, the VBM increased and CBM decreased by almost the same amount as in Ta atom substitution. Both of these two metal substitutions result in magnetic states due to the charge mismatch between W, Ta, and Hf atoms. However, in these cases, exchange splitting is much smaller than the bandwidth; hence, the resultant magnetic moments could be nonferromagnetic. Overall, magnetic moments in these cases would not add any extra factor to optical absorption.

Addition of an extra nitrogen atom as an interstitial impurity added to the substituted Ta or Hf atom creates a different interesting situation. For Ta (Fig. 15), the band gap is almost nonexistent for the majority spin, whereas for the minority spin, there is a gap of 1.12 eV. This situation could be an example of a half-metal. For Hf substitution with N atoms, there are gaps of 0.60 and 0.86 eV for the majority and minority spins, respectively. Because of the impurity bands due to the extra N atom and the structural deformation, there is a splitting of valence bands for both spin types. For Hf (Fig. 16), there is a greater exchange splitting of N *p* bands, 0.8 eV, which is large compared to the corresponding bandwidth. Also, although the collective valence band's upward shift is significant, the conduction-band shift is very small. A similar situation occurs when an extra O atom is used as an interstitial instead of a N atom. Note that for Hf (Ta), the extra O (N) has a half-filled, narrow, and high DOS at the Fermi level for the minority (majority) spin. As mentioned earlier, this type of behavior at the Fermi level causes further

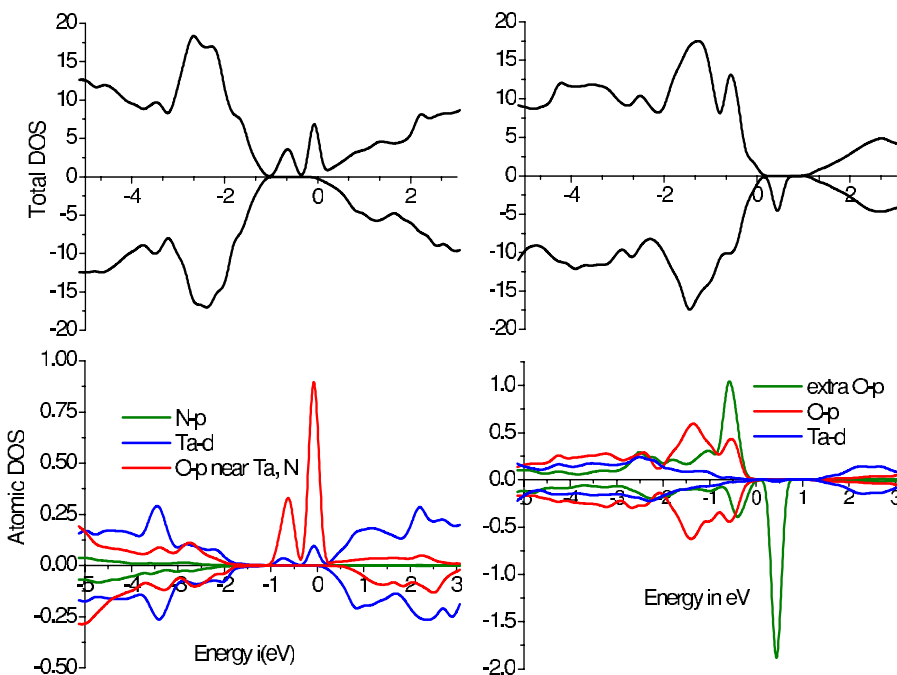


FIG. 15. (Color online) Total and local DOSs of WO_3 where a Ta atom was bonded with an extra interstitial N (left panel) or O (right panel) atom.

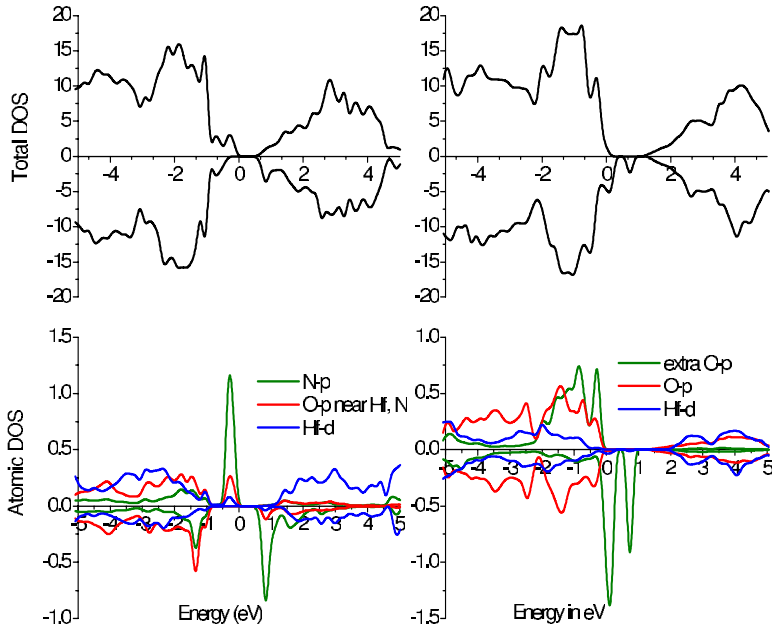


FIG. 16. (Color online) Total and local DOS of WO_3 where a Hf atom was bonded with an extra interstitial N (left panel) or O (right panel) atom.

electronic relaxation. This issue will be discussed in greater detail elsewhere. Interestingly, Ta+N and Hf+O in WO_3 make it a half-metal material and *p*-type material, respectively. Two other combinations, Ta+O and Hf+N, have fully occupied valence bands. In general, substitution of metal atoms may help to shift the band gaps when the substituted metal can add some ionicity to the system; however, adding interstitial impurity to it gives some extra control on its conductivity.

VI. CODOPING

We now discuss codoping in WO_3 to avoid the charge-mismatch situation. It was argued³⁴ that codoping can overcome the doping asymmetry in wide band semiconductors. In general, it may also help to reduce the recombination centers in the materials and hence would also help to increase the photocurrent. We have seen in the preceding discussion that single-anion or single-cation substitution creates unsaturated bonds that contribute to several distortions in the band structures. The overall band shape was undistorted only for Mo substitution but unfortunately, it did not raise the band edges at higher energies. Now, for N substitution, if one W atom bonded to a N atom is replaced by a Re atom, then Re-N would be isovalent to W-O, so no hole states would be expected. As expected from the total DOS plot (Fig. 17), the valence band is completely filled with no hole states, and the valence-band edge is an admixture of N *p* and O *p* bands with a contribution from Re *d* bands, which is expected from Table I. It also increased by 0.19 eV compared to the pure WO_3 valence band. However, the CBM, mainly composed of W *d* band, slightly decreased by about 0.09 eV. The minimum band gap, 1.03 eV, in this case is indirect at ($B \rightarrow \Gamma$).

On the other hand, for Ta atom substitution, if another F atom is substituted for O, then Ta-F would again be isovalent to the W-O dimer. Here, the band gap is direct at the Γ point and is 1.21 eV, which is slightly less than the WO_3 band gap.

The valence-band edge shifted upward by 0.09 eV and the conduction-band edge remained almost unchanged. The F atom *2p* band did not contribute to the VBM but rather, given its high electronegativity, started from 0.6 eV below the Fermi level and hybridized mainly with the *d* bands. Similar to Re-N codoping, the CBM mainly has the W *d* character. The Ta *d* band starts at an energy 0.20 eV higher

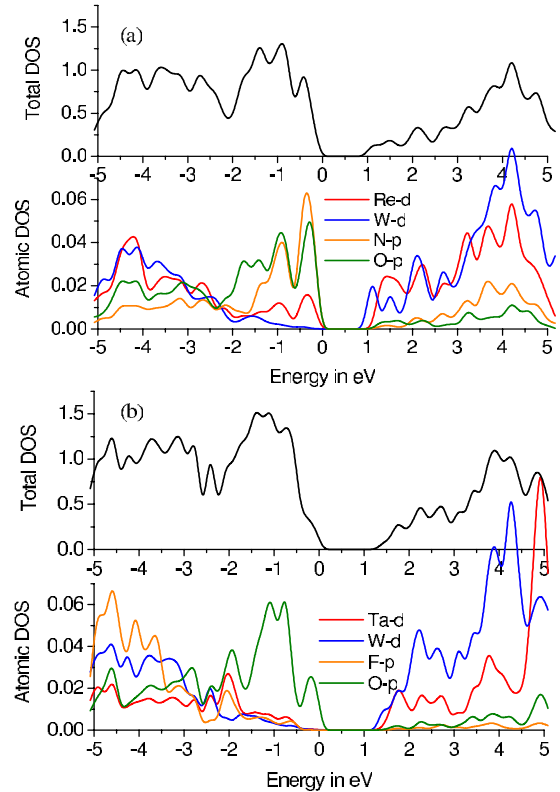


FIG. 17. (Color online) (a) Total and local DOS plot for Re-N codoped in WO_3 . (b) Total and local DOS plots for Ta-F codoped in WO_3 .

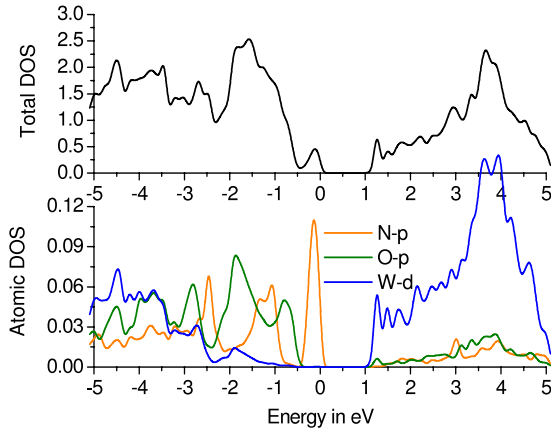


FIG. 18. (Color online) DOS plots for N-H substitutional codoping for O in WO_3 . The upper panel and the lower panel show total and site and angular momentum projected atomic DOSs, respectively.

than the conduction-band edge. The binding energy for the Re-N and Ta-F pair codopings are -2.24 and -1.02 eV, respectively. This shows the higher doping probability of the Re-N pair.

Similarly, an O atom can be substituted by a N atom with one H atom attached to it. As NH molecule would then be isovalent to O, the charge mismatch would be avoided and the recombination center could be reduced. The relaxed N-H distance, substituted for oxygen, was 1.05 Å. Here, due to the presence of an extra electron provided by the H atom, the partially filled N $2p$ band at the Fermi level from Fig. 2(b) is now completely filled, as seen in the DOS plot in Fig. 18. The ionic nature of the N-H bond is clear from the fact that the N $2p$ band near the Fermi level is not hybridized with the H $1s$ band. Here, this N $2p$ DOS is slightly detached, about 0.10 eV, from the rest of the valence band. This is expected because occupation by an electron would, in general, increase the energy of a band due to Coulomb repulsion. However, the resulting structure is significantly distorted, at least locally. The H $1s$ band negligibly contributes to the upper part of the valence band. Because N is less electronegative than O, this may suggest an upward lifting of the conduction band. We indeed found that the upward shift in energy for the valence and conduction-band edges are significant here, 0.57 and 0.16 eV, respectively. The band gap was found to be 0.89 eV, which is 0.42 eV less than the undoped WO_3 . One of the main features of this present configuration is that the H atom did not bond with the W atom as N did; rather, it extends out for the O atom on the other chain, and the O-H distance is 1.81 Å. The valence-band edge consists of O p and N p bands. The presence of the H atoms with N do not act the same way as O atoms do. It is interesting to compare the current result with only a N-atom substitution on O. The increase of the CBM is slightly higher here with extra H doping.

VII. FORMATION ENERGIES

Figure 19 shows the variation of formation energies in the limit of O-rich and W-rich conditions. The method of calcu-

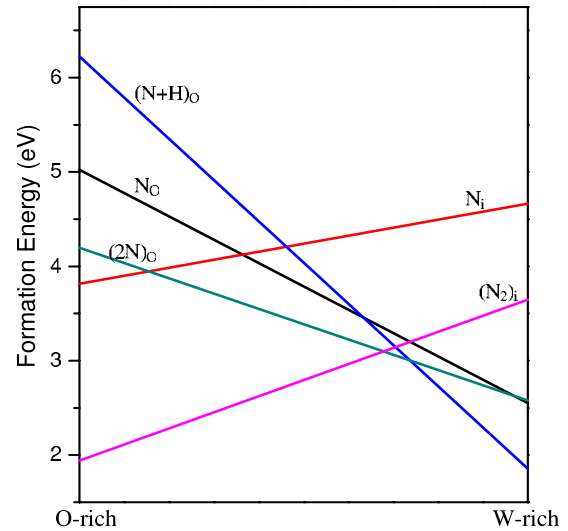


FIG. 19. (Color online) Formation energies of different defects at O-rich and W-rich conditions.

lating formation energies were discussed in detail in many reviews³⁵ and will not be discussed here. One point needs to be noted here: the N chemical potential is bounded at W-rich conditions by the WN_2 formation enthalpy, so that no undesirable W-N phase is formed at W-rich growth condition. As can be seen in Fig. 19, all the impurity formation energies strongly depend on the growth condition. We see that N_i is favorable than N_O at O-rich condition by 1.210 eV, whereas less favorable in the W-rich condition by 2.115 eV. Interestingly, two substitutional N atom (split interstitial) has a much lower formation energy than the one N-atom substitution at O-rich condition, however, has almost the same formation energy at W-rich condition. On the other hand, isovalent substitutional impurity $(\text{N}+\text{H})_O$ is more prone to form at the cation rich condition. Also, addition of N_2 at the A site [indicated as $(\text{N}_2)_i$ in Fig. 19] is more favorable than the substitutional N-type impurity except only near the cation rich growth condition. Also, N_2 formation at the A site has 1.874 eV less formation energy than single N interstitial at O-rich growth condition; the difference reduces to 1.023 eV at W-rich condition. The lower formation energy at both the extreme growth conditions suggests that interstitial N is most likely to be found as N_2 at the A position (Fig. 1).

VIII. OPTICAL ABSORPTION PROPERTIES

Figure 20 shows the optical absorption plot for two cases, $3N_i$ and $(\text{N}-\text{H})_O$, along with the undoped WO_3 case. These optical properties were calculated by the optic code³⁶ as implemented in WIEN2K.³⁷ For the optical plots in this paper, only the diagonal components of the momentum matrix were calculated because the off-diagonal elements would not significantly contribute. Also, these plots are for the non-spin-polarized cases because two of the structures [Figs. 20(a) and 20(c)] have no spin-magnetic moments; for the other case [Fig. 20(b)], no long-order magnetic moments are expected. Also, no band gap corrections were made for these absorption plots.

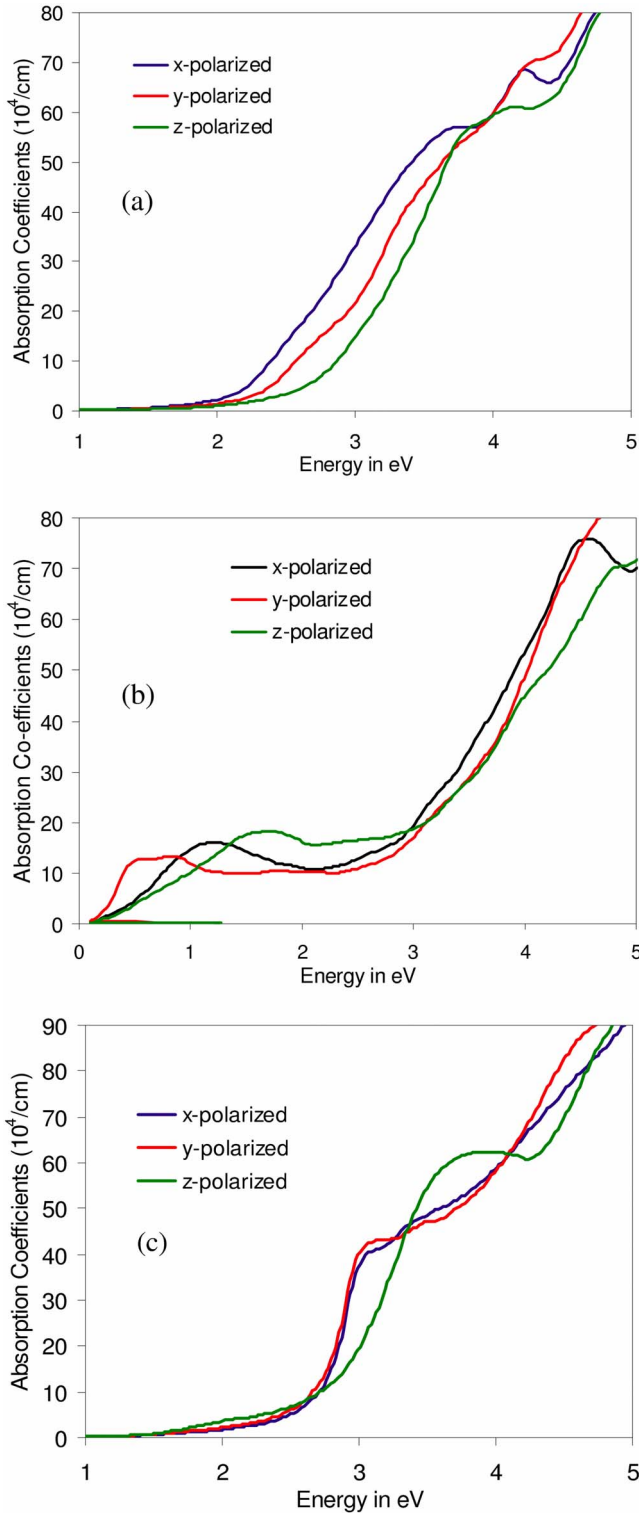


FIG. 20. (Color online) Optical absorption plots for (a) undoped, (b) three interstitial N impurities, and (c) N-H codoped WO_3 .

Figure 20(a) shows that the onset of the optical absorption is from below 2 eV. However, because the experimental gap is 2.62 eV, the real onset should be above that energy. At the calculated band gap, 1.31 eV, no transition is found mainly because, as mentioned before, that the gap is pseudodirect. So, the transition matrix has negligible values at the gap at Γ

point. For 3N interstitial impurity [Fig. 20(b)], it is clearly seen that the optical absorption sharply started at a very low energy, around 0.2 eV, with higher absorption coefficients. On the other hand, for N-H codoped WO_3 [Fig. 20(c)], the lower-energy absorption spectra are similar to that of the undoped WO_3 , which show the similarity of these two configurations due to isovalent substitution. However, at around 3 eV, the absorption coefficients sharply increase to $42 \times 10^4 \text{ cm}^{-1}$, whereas for the undoped and 3N interstitial cases, the absorption coefficients increase to 31×10^4 and $20 \times 10^4 \text{ cm}^{-1}$, respectively. Note that the absorption coefficients have values within 10×10^4 – $20 \times 10^4 \text{ cm}^{-1}$ for an energy range of 1.00–3.00 eV for the 3N interstitial impurity, whereas the NH codoping has slightly higher values below 2 eV than that of undoped WO_3 . Further addition of impurity is needed to enhance the lower end absorbance for the NH codoping case. At the higher energies, above 5.00 eV or more, all the absorption curves show a similar behavior. This shows that away from the fundamental gap, the band structures do not change much from that of the pure WO_3 .

IX. CONCLUSION

We have presented first-principles calculations of different atomic impurities in WO_3 and their electronic properties. These results would provide guidance for making WO_3 a suitable candidate for photoelectrodes for hydrogen generation by water splitting. A general way to reduce the band gap is to produce completely filled or partially filled impurity bands on top of the valence band. This was achieved by N substitution in WO_3 . We found that substitutional N impurities raise the valence-band maxima but do not have a significant impact on the conduction band of WO_3 . For interstitial N atom, a relatively better modification was observed, and the conduction band was affected. Impurity bands can be placed below the conduction band by placing an interstitial N bonded with an O atom. In general, substitutional or interstitial N impurity makes WO_3 a *p*-type or an *n*-type semiconductor, respectively. Especially for interstitial impurities, we found that a N_2 dimer placed in the hollow position (i.e., A site or the perovskite structure ABO_3) in the crystal has a very high binding energy for N-N dimer formation, and it has a significant effect compared to simple substitutional or interstitial N atom. Due to its relatively lower formation energy, formation of this defect is more favorable. In this case, although the band gap increased by few tenths of an eV, the conduction-band edge considerably increased in energy. In addition to N_2 at an A site, an interstitial N bonded with O significantly moves the band edges and reduces the band gap as well. Here, the conduction band increased by a tenth of an eV compared to the undoped WO_3 . We found that, consistent with the experimental results, the higher N-atom concentration reduced the band gap further. The higher N solubility in the host can be achieved by using the nonequilibrium growth technique. A smaller band gap (0.42 eV less than the undoped WO_3) and a significant band-edge shift were also obtained by NH substitution for O atom. The VBM and CBM shiftings were 0.57 and 0.16 eV, respectively. On the other hand, the conduction-band-edge shift was not very signifi-

cant for the metal-atom substitutions considered here. For example, Ta atom substitution did not give significant band-edge shifting. A similar situation was found for Hf substitution. Although metal-atom codoping such as Ta-F or Re-N is isovalent to W-O compound and is easily formed, it did not shift the conduction band as necessary, however, lower the overall band gap. Finally, among the impurities considered here, interstitial N₂ was found to be relatively more favorable. On the other hand, isovalent codoping, which would be necessary to reduce the carrier recombination centers, may be used as an initial doping stage, and then further doping

can be done to tune the band gap, band-edge positions, and carrier concentration in the materials.

ACKNOWLEDGMENTS

This work was supported by the U.S. Department of Energy through the University of Nevada Las Vegas Research Foundation under Contract No. DE-AC36-99-GO10337. This research used resources of the National Energy Research Scientific Computing Center, which is supported by the Office of Science of the U.S. Department of Energy under Contract No. DE-AC02-05CH11231.

*muhammad_huda@nrel.gov

¹O. Khaselev and J. A. Turner, *Science* **280**, 425 (1998).

²A. Fujishima and K. Honda, *Nature (London)* **238**, 37 (1972).

³T. Bak, J. Nowotny, M. Rekas, and C. C. Sorrell, *Int. J. Hydrogen Energy* **27**, 991 (2002).

⁴M. Grätzel, *Nature (London)* **414**, 338 (2001).

⁵B. Gao, Y. Ma, Y. Cao, W. Yang, and J. Yao, *J. Phys. Chem. B* **110**, 14391 (2006).

⁶S. K. Deb, *Appl. Opt.* **3**, 192 (1969); S. K. Deb, *Philos. Mag.* **27**, 801 (1973); S. K. Deb, *Sol. Energy Mater. Sol. Cells* **92**, 245 (2008).

⁷E. L. Miller, B. Marsen, B. Cole, and M. Lunn, *Electrochem. Solid-State Lett.* **9**, G248 (2006); Eric L. Miller, Daniela Paluselli, Bjorn Marsen, and Richard E. Rocheleau, *Sol. Energy Mater. Sol. Cells* **88**, 131 (2005).

⁸The position of CBM with respect to the H⁺/H₂O potential depends on the pH of the aqueous solution. Lower pH does reduce the energy gap between CBM and the H⁺/H₂O potential, but the electrodes may become unstable against the corrosion.

⁹H. Asahi, T. Morikawa, T. Ohwaki, K. Aoki, and Y. Taga, *Science* **293**, 269 (2001).

¹⁰K. Yang, Y. Dai, B. Huang, and S. Han, *J. Phys. Chem. B* **110**, 24011 (2006).

¹¹D. W. Hwang, J. Kim, T. J. Park, and J. S. Lee, *Catal. Lett.* **80**, 53 (2002).

¹²J. Tang and J. Ye, *J. Math. Chem.* **15**, 4246 (2005).

¹³P. Maruthamuthu, M. Ashokkumar, K. Gurunathan, E. Subramanian, and M. V. C. Sastri, *Int. J. Hydrogen Energy* **14**, 525 (1989).

¹⁴W. Erbs, J. DeSilvestro, E. Borgarello, and M. Grätzel, *J. Phys. Chem.* **88**, 4001 (1984).

¹⁵D. Paluselli, B. Marsen, E. L. Miller, and R. E. Rocheleau, *Electrochem. Solid-State Lett.* **8**, G301 (2005).

¹⁶S. B. Zhang and Su-Huai Wei, *Phys. Rev. Lett.* **86**, 1789 (2001).

¹⁷Y. Yan, S. B. Zhang, and S. T. Pantelides, *Phys. Rev. Lett.* **86**, 5723 (2001).

¹⁸The energies of the atomic orbitals were calculated by a LAPW code; see S.-H. Wei, H. Krakauer, and M. Weinert, *Phys. Rev. B* **32**, 7792 (1985).

¹⁹J. P. Perdew and A. Zunger, *Phys. Rev. B* **23**, 5048 (1981).

²⁰P. E. Blöchl, *Phys. Rev. B* **50**, 17953 (1994).

²¹G. Kresse and D. Joubert, *Phys. Rev. B* **59**, 1758 (1999).

²²G. Kresse and J. Hafner, *Phys. Rev. B* **48**, 13115 (1993).

²³G. Kresse and J. Furthmüller, *Comput. Mater. Sci.* **6**, 15 (1996).

²⁴G. Kresse and J. Furthmüller, *Phys. Rev. B* **54**, 11169 (1996).

²⁵G. A. de Wijs, P. K. de Boer, R. A. de Groot, and G. Kresse, *Phys. Rev. B* **59**, 2684 (1999).

²⁶M. Methfessel and A. T. Paxton, *Phys. Rev. B* **40**, 3616 (1989).

²⁷H. J. Monkhorst and J. D. Pack, *Phys. Rev. B* **13**, 5188 (1976).

²⁸B. T. Matthias, *Phys. Rev.* **76**, 430 (1949).

²⁹S. Reich, G. Leitus, Y. Tssaba, Y. Levi, A. Sharoni, and O. Millo, *J. Supercond.* **13**, 855 (2000).

³⁰A. Simon, *Angew. Chem., Int. Ed. Engl.* **36**, 1788 (1997).

³¹M. N. Huda, Y. Yan, S.-H. Wie, and M. M. Al-Jassim (unpublished).

³²The fundamental gap here is referred to as the actual gap that was between the occupied and unoccupied bands in undoped WO₃. Due to an N-atom impurity, the originally unoccupied conduction bands now become slightly occupied, so the gap here is basically between the occupied bands.

³³R. Vandenbosch, *Phys. Rev. A* **67**, 013203 (2003).

³⁴Y. Yan, J. Li, S.-H. Wei, and M. M. Al-Jassim, *Phys. Rev. Lett.* **98**, 135506 (2007).

³⁵For example, S.-H. Wei, *Comput. Mater. Sci.* **30**, 337 (2004); C. G. Van de Walle and J. Neugebauer, *J. Appl. Phys.* **95**, 3851 (2004).

³⁶C. Ambrosch-Draxl and J. O. Sofo, *Comput. Phys. Commun.* **175**, 1 (2006).

³⁷P. Blaha, K. Schwarz, G. K. H. Madsen, D. Kvasnicka, and J. Luitz, *WIEN2k, An Augmented Plane Wave Plus Local Orbitals Program for Calculating Crystal Properties*, (Technical Universität Wien, Austria, 2001).